MZUZU UNIVERSITY

DESIGN AND PERFORMANCE ANALYSIS OF GLUCOSE CONCENTRATION SENSOR BASED ON SILICON-ON-INSULATOR MICRORING RESONATOR

BY

LUGHANO MACHESO

A DISSERTATION SUBMITTED TO THE DEPARTMENT OF PHYSICS AND ELECTRONICS IN PARTIAL FULFILLMENT FOR THE REQUIREMENTS OF THE AWARD OF THE BACHELOR OF SCIENCE (HONOURS) DEGREE IN PHYSICS AND ELECTRONICS

JANUARY, 2024

Abstract

Integrated silicon photonics has become a relevant field for research in modern technology due to its promising platform for easy compatibility with Complementary Metal-Oxide Semiconductor (CMOS) fabrication processes. This has led to huge improvements in the design and implementation of chip-based photonic integrated circuits including microring resonators. In this study, a microring resonator has been designed and simulated by using the Finite Difference Time Domain (FDTD) algorithm in the software ANSYS Lumerical MODE Solutions. The designed microring resonator has the add-drop configuration whereby the ring waveguide is in between two parallel bus waveguides. Different concentrations of glucose ranging from 0-160 g/dl were considered to study the performance of the sensor. A change in the glucose concentration or refractive index causes a shift in the resonance wavelength. This shift in resonance wavelength is the principle upon which microring resonators function. The simulation results show an accurate approximation with other designed simulated results with the sensitivity value at 155.24 nm/RIU, quality factor at 446 and figure of merit at 51.7.

Table of contents

List of Figures

List of Tables

Chapter 1

Introduction

1.1 Background

Photonic Integrated Circuits (PICs) have over the years developed the integration of more diverse devices including active and passive components which range from light sources, detectors and amplifiers to beam splitters, gratings, couplers, polarizers and interferometers. These devices act as fundamental building blocks of more complex circuits which perform various functions on optical signals used in applications such as: optical communication, instrumentation as well as sensing. Silicon-on-insulator (SOI) waveguides are formed by growing a thick buffer layer of silicon oxide (SiO_2) on the silicon substrate, followed by a thin layer of silicon. The waveguide is then formed by lithographic patterning and dry etching. Afterwards, it is covered with another layer of silicon oxide (SiO2)[11].

In this modern age there is a high demand for higher bandwidth for processing signals at high speed. Unlike conventional electric circuits where signal processing is limited due to slow speed and large power consumption, the use of optical or photonic circuits is an alternate way that offers signal processing at a higher rate with low power consumption [12].

Photonic circuits use light instead of electricity which makes them 10 to 100 times faster and more energy efficient because they show lower heat loss, better signal-to-noise ratios and are less susceptible to interference than electrical systems. This property makes photonic circuits to be suitable for use in communication. Optical cavities such as waveguides can confine light in a small volume or space of a few nanometers causing a small change in the wavelength of the trapped light. This has led to the development of biosensors based on microring resonators [12].

The microring resonator (MRR) is a waveguide that is looped back to itself in order to achieve resonance when optical path length is equivalent to whole number or integral multiple of wavelengths. This property enables the microring resonator to offer the function of wavelength selectivity as compared to splitters, combiners and the interferometer. Light is propagated in the waveguide by interfering with itself through the total internal reflection phenomenon. Microring resonators are widely used in modern technologies for the construction of optical devices such as switches, filters, logic gates, differential amplifiers, delay lines and sensors[3].

Recent research advances have shown that microring resonators can be configured in two ways as; lateral geometry whereby the resonator is comprised of a single or double waveguide coupled to a circular ring and are situated on the same plane or vertical geometry in which the ring waveguide is placed above the bus waveguide(s). In this study, the microring resonator has the lateral geometry because with this configuration the resonator's performance can be easily enhanced by reducing the gap between the ring and bus waveguide. However, this design can be limited by fabrication constraints [6].

Optical ring resonators rely on the light-matter interaction to convert the presence of biological or chemical parameters into measurable optical signals. In the sensing technology, ring resonators have unique advantages compared to traditional sensors where the light-matter interaction length is basically the sensor's physical length. With optical ring resonators, the circulating nature of the resonant modes creates a longer light-matter interaction length which mainly depends on the resonator's configuration. Hence, despite having a small physical size, ring resonators have an effective interaction length of a few tens of centimeters and are able to offer better sensing performance with small footprint whilst using a small analyte amount[22].

There are mainly two kinds of sensing that ring resonators can perform depending on analyte positioning. These are surface sensing and bulk sensing. In bulk detection or sensing, signals result from the optical change in refractive index which is induced by the presence of the analyte in the entire region of the evanescent field and is proportional to the analyte concentration. This kind of sensing lacks detection specificity and is therefore mostly used to characterize the sensing performance of the ring resonator. During surface sensing signals come from analytes in close proximity to the resonator's surface. The capture molecules are immobilized on the sensors surface to provide detection specificity. The spectral shift in wavelength is generated when the analytes are bound to the capture molecules which changes the refractive index near the surface[22].

There are three sources of propagation loss in the waveguides which are optical absorption in the core and cladding materials, electromagnetic scattering and radiation leakage. Losses due to optical absorption may arise from electronic processes such as atomic and molecular vibrations in glass (SiO_2) and interband and intraband transitions in semiconductors. Secondly, losses due to electromagnetic scattering are caused by Rayleigh scattering and surface roughness scattering. In Rayleigh scattering, light is scattered by small fluctuations in the refractive index resulting from defects or contaminants in the material. This type of scattering decreases with wavelength by λ^{-4} and it is usually much smaller than the latter. Surface roughness scattering is caused by the fabrication process such as deposition and etching. There is a larger scattering loss at the waveguide sidewalls than at the top and bottom surfaces of the waveguide core which may be caused by index contrast and confinement strength of light in the waveguide. Thirdly, waveguide losses due to radiation leakage result from bending loss and substrate leakage. Bending loss takes place in curved waveguides and it exponentially depends on the bending radius. Because of the high-index contrast of the SOI material system, bending loss remains low for tight bends with radii down to 2.5 micrometers. Substrate leakage occurs when light from a waveguide leaks into a high-index substrate. The evanescent field of a waveguide extends into the under cladding. The high-index substrate in this case silicon, causes evanescent coupling of light into the substrate which then radiates away as loss. However, this can be minimized by increasing the thickness of the under cladding layer in order to provide enough space between the waveguide core and the high-index substrate[23].

In integrated optical devices coupling can take place in two ways; through evanescent field coupling between modes of two adjacent waveguides or through coupling between modes of the same waveguide due to periodic index perturbations. However, directional couplers are the fundamental building block of microring resonators and as such, MRRs operate based on the principle of evanescent field coupling. The ring resonator is basically constructed by feeding one output of a directional coupler back into its input. The directional coupler functions on the principle of the coupled mode theory which is an analytical method for studying coupled optical waveguides and their modes. The coupled mode theory is implemented for the analysis of mode coupling whereby the interaction of the evanescent fields of neighboring waveguides leads to transferring of light from one waveguide to the other or when light is coupled between modes of the same waveguide due to index perturbations. Light in microring resonators is coupled into the ring waveguide due to the evanescent field between modes of the ring waveguide and the bus waveguides. The amount of light that is distributed among the waveguides during coupling depends on the coupling length and coupling gap. The waveguides support the propagation of modes with specific configurations of the electric and magnetic fields which are also solutions of the Maxwell's equations with boundary conditions. These modes propagate along the waveguide with a phase change defined by the corresponding propagation constants. For silicon on insulator waveguides, analytical solutions may not be possible and numerical techniques such as Finite Difference Time Domain (FDTD) can be employed to study the modes of the waveguides[20].

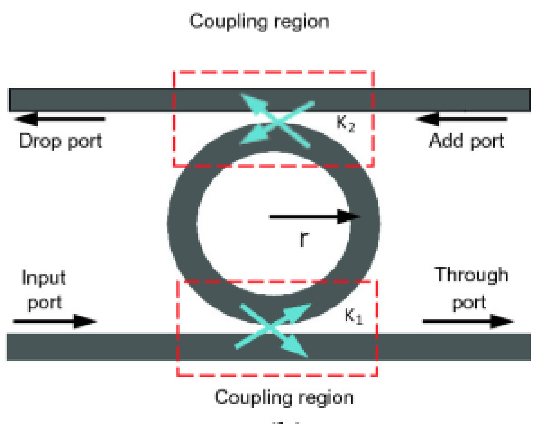

Figure 1.1: MRR coupling regions

Figure 1.1 shows the coupling regions between the bus and ring waveguides. During coupling a condition called critical coupling must be achieved in order to obtain high extinction ratio of the cavity resonance. This takes place when coupling loss between the ring and bus waveguides is equivalent to the propagation loss inside the ring and the wavelength of the laser is tuned to a cavity mode of the ring. The bus waveguide may be terminated by a photodetector at the other end so that at critical coupling little or no light travels past the ring to the photodetector[15].

The Silicon-on-insulator microring resonators are highly manufacturable as the transmission spectrum mainly depends on the resonators surrounding and they can be made with a large quality factor, large extinction and low insertion loss. Secondly, they can be produced compactly, thus allowing several resonators to be embedded on a single chip. This permits simultaneous measurements of multiple analyte concentrations. Thirdly, they can be made cheap when fabricated with Complementary Metal-Oxide Semiconductor (CMOS) compatible processes in high volumes so that the sensor chips are disposable hence avoiding complex cleaning of the sensor surface after a single use. Receptor molecules that are selective to the analyte are immobilized on the resonator prior to the measurement by chemically modifying its surface. Firstly, an aqueous buffer solution is spread over the sensor surface to determine the reference resonance wavelengths that are equivalent to the optical path length of the resonator. Secondly, the test solution is then spread over the resonator, permitting the analyte molecules to bind to the immobilized receptors. The bound analyte molecules typically have a refractive index of 1.45 and replace water with a lower refractive index of 1.31. The resulting change of the effective roundtrip length causes an increase of each resonance wavelength equivalent to the number of binding events. By studying the transmission spectrum of the resonator repeatedly with a tunable laser and measuring the resonance wavelength shift as a function of time, the analyte's concentration can be determined[5].

In recent years, the rapid increase in using integrated photonic devices such as the MRR for biosensing applications has become of great interest. It is important that glucose sensors are highly sensitive and can provide accurate results of glucose concentration in low response time. Most existing glucose sensors utilize enzymes such as glucose oxidase (GOD). This acts as a catalyst by accelerating the reaction rate of the metabolic processes. It is used when glucose reacts with oxygen to produce gluconic acid ($C_6H_{12}O_7$) and hydrogen peroxide (H_2O_2). The analyte (blood) is sensed by the bio receptors that consist of enzymes on their surface. The receptor produces a signal when in contact with the surrounding stimuli and it sends this signal to the transducer. The transducer is used to convert one form of energy into another form of energy, in this case, from chemical energy to electrical energy. The electrical signal then goes to the detector which is connected to the device used for receiving final output data [13].

In essence, microring resonators detect the parameter or analyte based on the different properties of light like absorption, reflection and transmission. The light-matter interaction causes changes in the aforementioned properties of light due to change in the refractive index of the interacting surface. One advantage of optical biosensors is that they are non-electrical in nature. This enables them to analyze parameters by simply varying the wavelength of the light [1].

In this study, a highly sensitive microring resonator was designed to acquire results in low response time of glucose concentrations compared to conventional biosensors. Different concentrations of glucose in blood were considered to study the performance of the sensor based on key sensor parameters.

1.2 Problem Statement

Recent research on microring resonator-based biosensors mainly focuses on the enhancement of the sensors sensitivity without taking into consideration of equally important sensor parameters which are figure of merit, quality factor, Full Width at Half Maximum (FWHM) as they directly affect the analytes concentration in this case the glucose and can be used to review the sensors effectiveness.

1.3 Main Objective

The main objective of this study is to simulate a silicon on insulator microring resonator which is compact in size and can be employed for biosensing applications specifically in the detection of glucose levels.

1.4 Specific Objectives

The specific objectives of this study were to:

1. To calculate the sensitivity of the microring resonator in detecting very low concentrations of glucose.
2. To measure the Quality factor (Q-factor) of the microring resonator glucose sensor.
3. To analyze the Electrical and Magnetic field properties of the microring resonator glucose sensor.
4. To calculate the Figure of Merit (FOM) of the microring resonator glucose sensor.

Chapter 2

Literature Review

2.1 Review of relevant existing literature

In the early years, multiple laboratory tests had to be carried out over a period of time to determine glucose concentrations. Rapid development in biosensor technology has and is continuing to play a key role in providing an easy way to detect glucose. The biosensing market is growing rampantly as manufacturers are competing with several researches being carried out through simulations and experiments in order to enhance the sensitivity of biosensors such as the SOI microring resonators. The first glucose biosensor was proposed by Clark and Lyons in 1962. It became successful for commercial use in 1975 under the Yellow Springs Instrument Company and was named Model 23A YSI analyzer. It was based on the amperometric detection of hydrogen peroxide but was limited to use in clinical laboratories because it was expensive due to high cost of platinum electrode. However, the main challenge with the first biosensors was that they required a high operation potential to offer high selectivity. Over the years, significant efforts have led to the use of optical biosensors that offer high sensitivity at low operating potentials [24].

Many studies have been reported on the simulation of MRR [9], simulated an add-drop microring resonator using 3D FDTD method which consumes a lot of time and power and realized a sensitivity value of 120nm/RIU. Similarly, [14] also simulated a microring resonator using the 3D FDTD method. The sensor's figure of merit and free spectral range were not accounted for and the sensitivity value was 69 nm/RIU which can be optimized to detect changes at lower glucose concentrations by adjusting the geometric parameters of the MRR in order to obtain a high-quality factor since there is linearity between the quality factor and sensitivity of the MRR. [2] found sensitivity values of 79.7nm/RIU and 70.32 nm/RIU for two microring resonator simulations with glucose concentrations as the analyte. However, the details of the sensor's figure of merit, quality factor and free spectral range were not reported.

2.2 Fabrication of Microring Resonators

Fabrication technologies that are used to realize micro resonators have significantly evolved over the years. Recent advances in SOI MRR fabrication utilise wafers. This is carried out in three main stages: the wafer preparation, lithography and etching [8].

In the first stage, a semiconductor crystal such as silicon is transformed into a thin-flat wafer with a smooth surface. The wafer preparation involves various stages that are: crystal growth, wafer slicing, polishing and cleaning. During crystal growth, a high-quality semiconductor crystal is produced by melting silicon in a crucible and cooling it to a temperature of near its freezing point. Afterwards a mono crystalline ingot of uniform crystal structure is produced. Once the crystal is formed, it is sliced into thin wafers through a process known as wafer slicing. A wire saw is used to cut the crystal ingot into wafers of uniform thickness that usually range from a few hundred micrometers to over a millimeter. These wafer slices undergo a series of polishing steps to smoothen the surface like mirrors. This step is necessary because any surface imperfections can affect the performance of the semiconductor devices. After polishing, the wafers are thoroughly cleaned in order to eliminate any chemical residues. Ultrasonic cleaning methods are employed in this process in which the wafer is immersed in a cleaning solution and subjected to ultrasonic vibrations. Other cleaning methods use plasma to remove contaminants from the wafer surface [17].

The second stage is called lithography or photo lithography. In this stage the wafer is uniformly covered in a thick liquid called a photoresist. The coating is light-sensitive and is applied onto the wafer as it rotates through a spin-coating technique. Afterwards, a photo mask that consists of the resonator structure is then imaged on the resist by radiation exposure. The mask is positioned between the wafer and Ultra-Violet (UV) light source making sections of the wafer to be chosen for exposure. A series of lenses are placed between the mask and wafer so that as the UV light penetrates through the mask, the image can be easily transferred to the wafer [7].

There are various types of lithography techniques that range from optical to electron (ion) beam. The resolution of a lithography technique is mainly limited by the imaging property of the corresponding operating wavelength. Normally polymer is used as the photoresist because of its remarkable sensitivity to light exposure. When exposed to UV light, the photoresist (polymer) hardens and remains on the wafer while the unexposed photoresist is removed by a developing solution. The developing solution helps to preserve the imaged resonator pattern while removing the excess unexposed resist [7, 8].

In the final stage known as etching, the resonator pattern is transferred to the wafer through the removal of all material that is not protected by the resist with the use of etchants. Etching can be isotropic in which the material is removed uniformly in all directions or anisotropic in which the material is removed uniformly in the vertical direction [18].

There are two kinds of etching, namely, dry etching and wet etching. Wet etching is a process that involves the use of liquid chemicals to remove materials from the wafer. During this process, all materials that are not covered by the mask are etched away by the liquid chemicals while dry etching involves the use of plasma or etchant gasses to remove the substrate material. The reaction can be done by using high kinetic energy of particle beams, chemical reaction or a combination of both [18]. Some of the commonly used gases in dry etching are methane (CH4), nitrogen (N2), silicon tetrachloride (SiCl4) and argon (Ar)[21].

2.3 Ring Resonator Performance Parameters

2.3.1 Quality factor

The Quality factor (Q-factor) is a measure of the resonator capacity to circulate and store light. It is the ratio of the energy stored to the energy dissipated in the resonator. Q-factor can also be defined as a measure of the sharpness of the resonance relative to its central frequency. The Q-factor is calculated by using the equation:

$$Q = \frac{\lambda_{\mathrm{res}}}{FWHM} \tag{2.1}$$

where λ_{res} is the resonant wavelength and FWHM is the Full Width at Half Maximum.

2.3.2 Full Width at Half Maximum

The Full Width at Half Maximum (FWHM) is a measure that represents the width of a curve measured between the two points where the curve's value is half its maximum. It is given by the equation:

$$FWHM = \frac{k^2 \lambda^2}{\pi n_{\mathrm{eff}} L} \tag{2.2}$$

where λ is the optical wavelength and k is the cross-coupling coefficient.

2.3.3 Free Spectral Range

The Free Spectral Range (FSR) is defined as the separation distance between two adjacent resonant wavelengths. This is given by:

$$FSR = |\lambda_{\mathrm{res},1} - \lambda_{\mathrm{res},2}| \tag{2.3}$$

or

$$FSR = \frac{\lambda^2}{n_g L} \tag{2.4}$$

where n_g is the group index

2.3.4 Finesse

Finesse (F) is defined as the ratio of the FSR and the FWHM. It is a measure of the sharpness of resonances relative to their spacing.

$$F = \frac{FSR}{FWHM} \tag{2.5}$$

This has a physical interpretation of the number of round trips of light before its intensity or energy in the MRR decays to 1/e of its initial value [5, 8].

During resonance, the wavelength of light fits a whole number of times inside the optical length of the ring or the phase ϕ is a multiple of 2π. This is expressed as:

$$\lambda_{\text{res}} = \frac{n_{\text{eff}} L}{m}, m = 1, 2, 3 \ldots \tag{2.6}$$

where L is the optical path length, n_{eff} is the effective refractive index and m is the mode number.

The MRRs performance in detecting glucose is identified by the sensitivity value. The equation for calculating sensitivity is given by:

$$S = \frac{\Delta\lambda_{\text{res}}}{\Delta n} \tag{2.7}$$

where $\Delta\lambda_{\text{res}}$ is the change in resonant wavelength and Δn is the change in refractive index units.
The microring resonator sensor‘s figure of merit will be calculated by using the equation:

$$FOM = \frac{S}{FWHM} \tag{2.8}$$

The main purpose of this study is to increase the sensitivity of the basic add-drop microring resonator by simulating using the FDTD method in Lumerical software MODE Solutions.

Chapter 3

Materials and Methods

3.1 Brief Description of Materials to be used

3.1.1 Ring Structure

The ring waveguide is coupled to two parallel bus waveguides. The incident field is transmitted to the drop port as illustrated in Figure 3.1

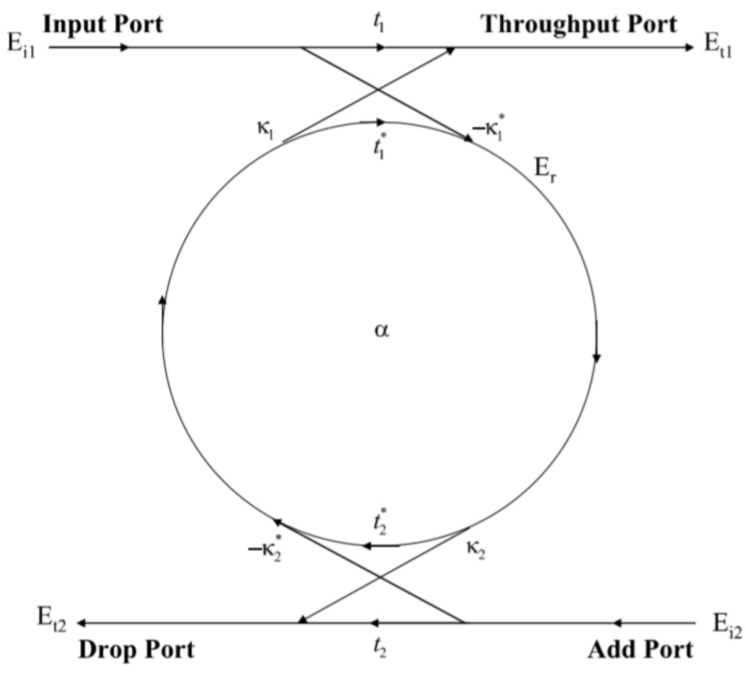

Figure 3.1: Add-drop ring resonator

3.1.2 Design of the Microring resonator

A 2D rectangular substrate of silicon oxide (SiO_2) was used for the realization of the sensor with silicon as the waveguide material. It consisted of a ring waveguide configured in lateral geometry to two parallel waveguides with a small gap between the two. Table 3.1 shows the following dimensions of the designed microring resonator: ring radius (R), gap (g), waveguide height (h), waveguide width (W) and base angle. These dimensions were utilised in order to achieve high FSR for better sensing performance and to reduce bending losses in the waveguide structure. Table 3.2 shows the sensor parameters that were used during simulation.

Table 3.1: MRR Dimensions

MRR Geometry	**Dimension**
Ring radius	3.1µm
Gap	0.1µm
Waveguide width	0.4 µm
Waveguide height	0.18 µm
Base angle	90

Table 3.2: Sensor parameters for the simulation

Symbol	**Significance**	**Unit**
$\boldsymbol{\alpha}$	Propagation loss	/m
$\boldsymbol{\beta}$	Propagation constant	Rad /cm
$\boldsymbol{\lambda}$	Optical Wavelength	nm
$\boldsymbol{k}$	Cross-coupling coefficient	
$\boldsymbol{t}$	Straight-through coupling coefficient	
$\mathbf{n_g}$	Group refractive index	
$\mathbf{n_{eff}}$	Effective refractive index	
$\mathbf{L_c}$	Coupling length	cm

The glucose concentrations used were of the range 0-160 g/dl with the simulation wavelength at 1548 nm which is optimal for photonic devices. This range was utilised to study the performance of the sensor below and above the normal blood glucose level in human beings which ranges between 70 and 130 g/dl. Table 3.3 shows the glucose concentration levels with their refractive indices.

Table 3.3: Refractive indices of glucose concentrations

Refractive Index	**Glucose concentration (g/dl)**
1.3101	0
1.3125	20
1.3149	40
1.3172	60
1.3196	80
1.3220	100
1.3244	120
1.3267	140
1.3291	160

The Finite Difference Time Domain (FDTD) method was used to analyze the structure in Ansys Lumerical MODE Solutions. The FDTD method or Yee's algorithm calculates the optical modes of the waveguide by solving Maxwell's equations on a cross sectional mesh of the waveguide. The polarization of guided light has a great influence on the light-matter interaction in the waveguide structure. The FDTD algorithm is one of the most preferred method because it is an advanced numerical analysis technique for computing the field distribution inside the resonator. It does not solve integral equations and can extract frequency domain data from the time domain results. FDTD is mainly based on the direct resolution of the Maxwell's equations in their differential form. This enables FDTD to simulate the behavior of electromagnetic (EM) waves in any kind of medium. The following derivations of equations are used for microring resonators [4].

$$\boldsymbol{\nabla}.\left(\varepsilon(\vec{r})\vec{E}(\vec{r},\vec{t})\right) = 0 \tag{3.1}$$

$$\boldsymbol{\nabla}.\left(\vec{H}(\vec{r},\vec{t})\right) = 0 \tag{3.2}$$

$$\boldsymbol{\nabla} \times \left(\vec{E}(\vec{r},\vec{t})\right) = -\mu_o \frac{\partial}{\partial t}\left(\vec{H}(\vec{r},\vec{t})\right) \tag{3.3}$$

$$\boldsymbol{\nabla} \times \left(\vec{H}(\vec{r},\vec{t})\right) = -\varepsilon_o \varepsilon(\vec{r}) \frac{\partial}{\partial t}\left(\vec{E}(\vec{r},\vec{t})\right) \tag{3.4}$$

Maxwell's equations are approximated to their finite differences. The curl equations are then evaluated by their vector components. The equations which are considered for the propagation of light in a medium are the curl equations:

$$\nabla \times \vec{E} = -\mu \frac{\partial H}{\partial t} \text{(Faraday's Law)} \tag{3.5}$$

$$\nabla \times \vec{H} = J + \varepsilon \frac{\partial E}{\partial t} \text{(Ampere's Law)} \tag{3.6}$$

All the equations are in a single direction as follows:

$$\frac{\partial H_x}{\partial t} = \frac{1}{\mu}\left(\frac{\partial E_y}{\partial z} - \frac{\partial E_z}{\partial y}\right) \tag{3.7}$$

$$\frac{\partial H_y}{\partial t} = \frac{1}{\mu}\left(\frac{\partial E_z}{\partial x} - \frac{\partial E_x}{\partial z}\right) \tag{3.8}$$

$$\frac{\partial H_z}{\partial t} = \frac{1}{\mu}\left(\frac{\partial E_x}{\partial y} - \frac{\partial E_y}{\partial x}\right) \tag{3.9}$$

$$\frac{\partial E_x}{\partial t} = \frac{1}{\varepsilon}\left(\frac{\partial H_z}{\partial y} - \frac{\partial H_y}{\partial z}\right) \tag{3.10}$$

$$\frac{\partial E_y}{\partial t} = \frac{1}{\varepsilon}\left(\frac{\partial H_x}{\partial z} - \frac{\partial H_z}{\partial x}\right) \tag{3.11}$$

$$\frac{\partial E_z}{\partial t} = \frac{1}{\varepsilon}\left(\frac{\partial H_y}{\partial x} - \frac{\partial H_x}{\partial y}\right) \tag{3.12}$$

The transverse magnetic (TM) and transverse electric (TE) modes are used for optical transmission. Both of the fundamental modes of TM and TE are commonly used. In the fundamental TE mode, the transverse electric field component is dominant and lies parallel to the direction of propagation of light while in the fundamental TM mode, the transverse magnetic field component is dominant and parallel to the direction of propagation of light. The TM modes shows better light-matter interaction but there are high optical losses. It is for this reason that the TE mode is instead preferred for optical devices [21].

In case of TE polarization, only the electric field components lie parallel to the resonator and magnetic field components that lie in the plane of the resonator have non-zero values. All other components (electric and magnetic) equal to zero.

$$\frac{\partial H_x}{\partial t} = \frac{1}{\mu}\left(- \frac{\partial E_z}{\partial y}\right) \tag{3.13}$$

$$\frac{\partial H_y}{\partial t} = \frac{1}{\mu}\left(\frac{\partial E_z}{\partial x}\right) \tag{3.14}$$

$$\frac{\partial E_z}{\partial t} = \frac{1}{\varepsilon}\left(\frac{\partial H_y}{\partial x} - \frac{\partial H_x}{\partial y}\right) \tag{3.15}$$

Likewise in the case of TM polarization, only magnetic field components lie parallel to the resonator and electric field components that lie in the same plane as the resonator have non-zero values. All other components (electric and magnetic) equal to zero.

$$\frac{\partial E_x}{\partial t} = \frac{1}{\varepsilon}\left(\frac{\partial H_z}{\partial y}\right) \tag{3.16}$$

$$\frac{\partial E_y}{\partial t} = \frac{1}{\varepsilon}\left(-\frac{\partial H_z}{\partial x}\right) \tag{3.17}$$

$$\frac{\partial H_z}{\partial t} = \frac{1}{\mu}\left(\frac{\partial E_x}{\partial y} - \frac{\partial E_y}{\partial x}\right) \tag{3.18}$$

FDTD calculates the electric and magnetic fields at every mesh point within the system and as they develop with time, this helps to provide details on how the EM wave moves through the model and to determine if the the model is working correctly.

The basic idea behind Yee's algorithm is to use central differences on a staggered grid (both in space and time). The resulting cell in two and three dimension is presented as shown in Figure 3.2

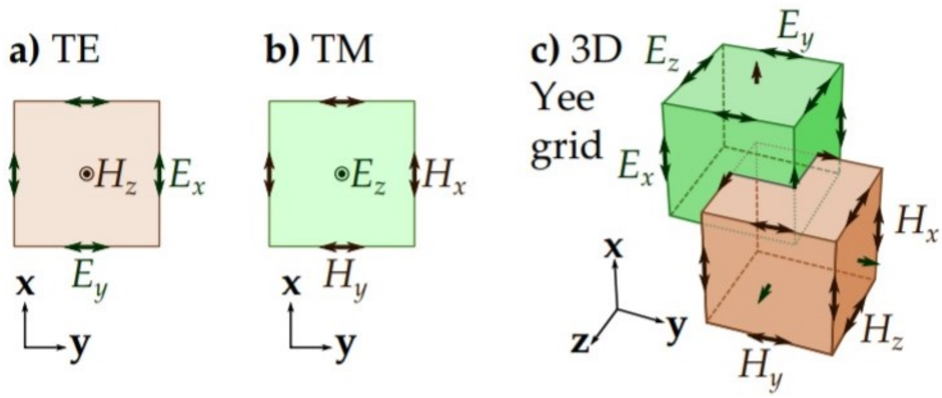

Figure 3.2: Yee cell in 2D and 3D

Problems dealing with wave propagation in which involve solutions that are oscillating and decaying with distance r. By simply truncating the grid with periodic boundary conditions, may lead to the slow decays causing artifacts from boundary reflections. The oscillation means that any real coordinate remapping from an infinite to a finite domain will result in solutions that oscillate infinitely fast as the boundary is approached. Such fast oscillations cannot be represented by a finite grid, and will instead form a reflecting hard wall. This problem can be solved by using an absorbing boundary layer. This layer is an artificial absorbing material that is placed adjacent to the edges of the grid. When a wave enters the absorbing layer, it is attenuated by the absorption and decays exponentially. In cases where the wave reflects off the boundary, the returning wave after one round trip through the absorbing layer is exponentially tiny. However with this approach the challenge is that, whenever the wave transitions from one medium to another such as the transition from non-absorbing to absorbing material, the wave reflects and instead of having reflections from the grid boundary, the wave will reflect from the absorbing boundary [16].

Perfectly Matched Layer (PML) boundaries are used during the simulation of resonators to absorb the impacted EM energy that falls on them, allowing the radiation to propagate out of the specified mesh region without interfering with the internal electric field [19]. Figure 3.3 illustrates the working of the perfectly matched layer.

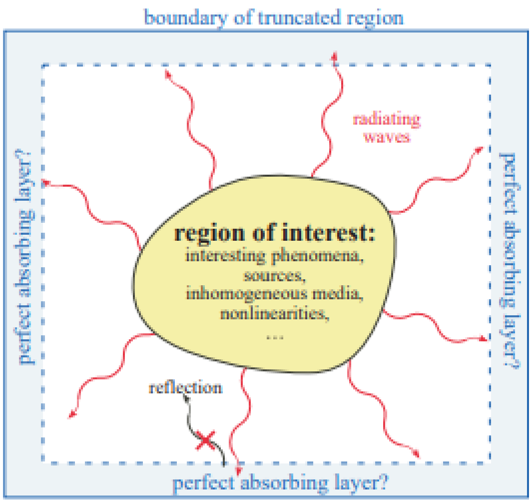

Figure 3.3: Perfectly matched layer

Chapter 4

Results and Discussion

The MRR simulation was set to 10000 fs to have a detailed calculation from the FDTD method. The default auto mesh feature was used in which the mesh configuration is non-uniform to minimize the effect of numerical dispersion. The mesh accuracy was set to 4 as this produces a good trade off between accuracy, memory requirements and simulation time. At the start, the simulation was run with the refractive index of 1.3101 (water) which has zero concentration of glucose at a temperature of 300K. This condition is suitable as it imitates the real conditions of experimental work for quality factor measurement. Figures 4.1 and 4.2 show the geometry of the designed MRR from different views.

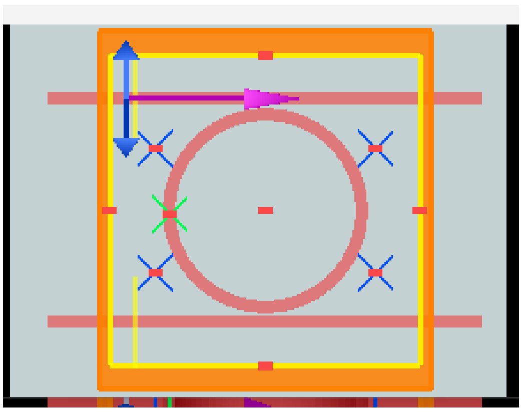

Figure 4.1: XY view

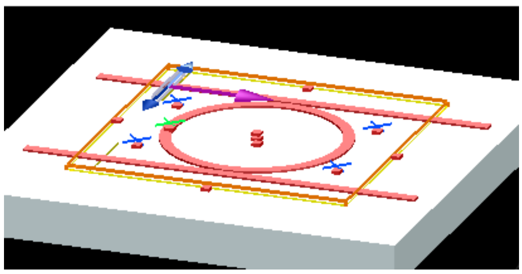

Figure 4.2: Perspective view

Figure 4.3 shows how light is coupled in the ring resonator waveguide. This was obtained by using the profile monitor which records the field profile in the frequency domain from simulation results across some spatial region within the simulation in the FDTD. The insert shows the electric field distribution of the x cross section.

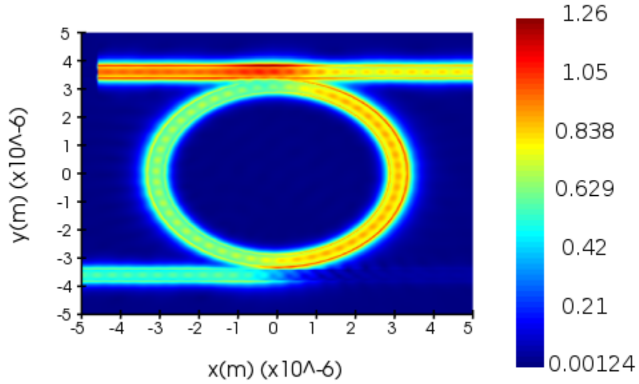

Figure 4.3: Profile Monitor for the Electric Field

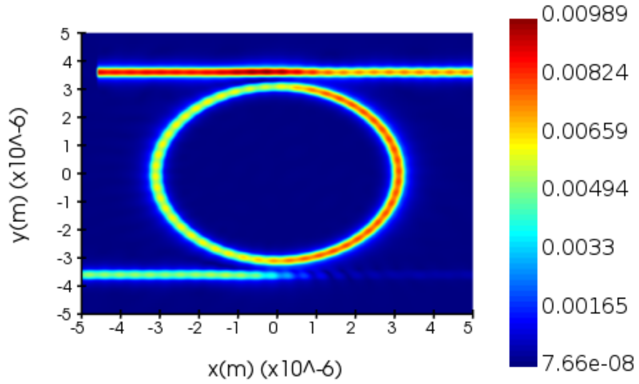

Figure 4.4: Profile Monitor for the Magnetic Field

Similarly, Figure 4.4 is showing the magnetic field profile. It can be observed from the magnetic field distribution that the intensity is less than that of the electric field. This is typically due to the use of dielectric materials in which the electric field tends to exist for a long time.

Figure 4.5 shows the transmission spectrum of the light at the through and drop ports. This was obtained by placing in monitors at the drop and through ports in order to capture the light spectrum from 1500 nm to 1600 nm whereby the attenuation rate is less within this wavelength range.

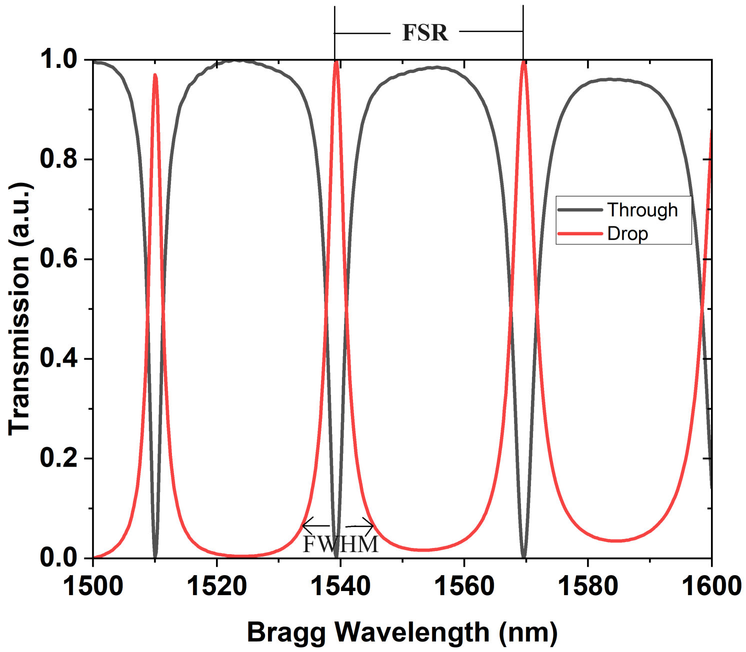

Figure 4.5: Transmission at through and drop ports

The FSR and Q-factor were calculated by using eqns (2.3) and (2.1) and were found to be about 29 nm and 446.96 respectively. The FWHM value was found to be 3.5 nm. The gap size between the bus waveguide and ring waveguide as well as the ring radius affect the quality factor and FSR, because the Q-factor increases with an increase in the radius and FSR decreases with the increasing radius. The Q-factor in the microring resonator is relatively low. This is a result of the small ring radius and strong coupling between the ring and bus waveguides. The Q-factor represents the number of oscillations of the field before the circulating energy is depleted to 1/e. When coupling the ring to the bus waveguides losses are introduced which can to decrease in the Q-factor. Therefore, in order to increase the Q-factor, it is essential to reduce the losses in the cavity. These losses can be reduced by the use of high quality SOI material and high quality fabrication processes. The Q-factor can also be increased by using a resonator with a large optical path length L, in addition to a small cavity loss. However, a large optical path length leads to lower finesse. In this study the finesse was calculated to be 8.23 using the eqn (2.5).

Figure 4.6 shows the transmission spectrum of the different concentrations of glucose.It can be observed that as the glucose concentration levels are increasing, the refractive index is also increasing leading to an increase in the resonant wavelengths. Hence, there is a shift in the resonant wavelength which denoted by $\Delta\lambda_{\text{res}}$. This has been further illustrated in Figure 4.7 which shows the bragg wavelength against the refractive index units.

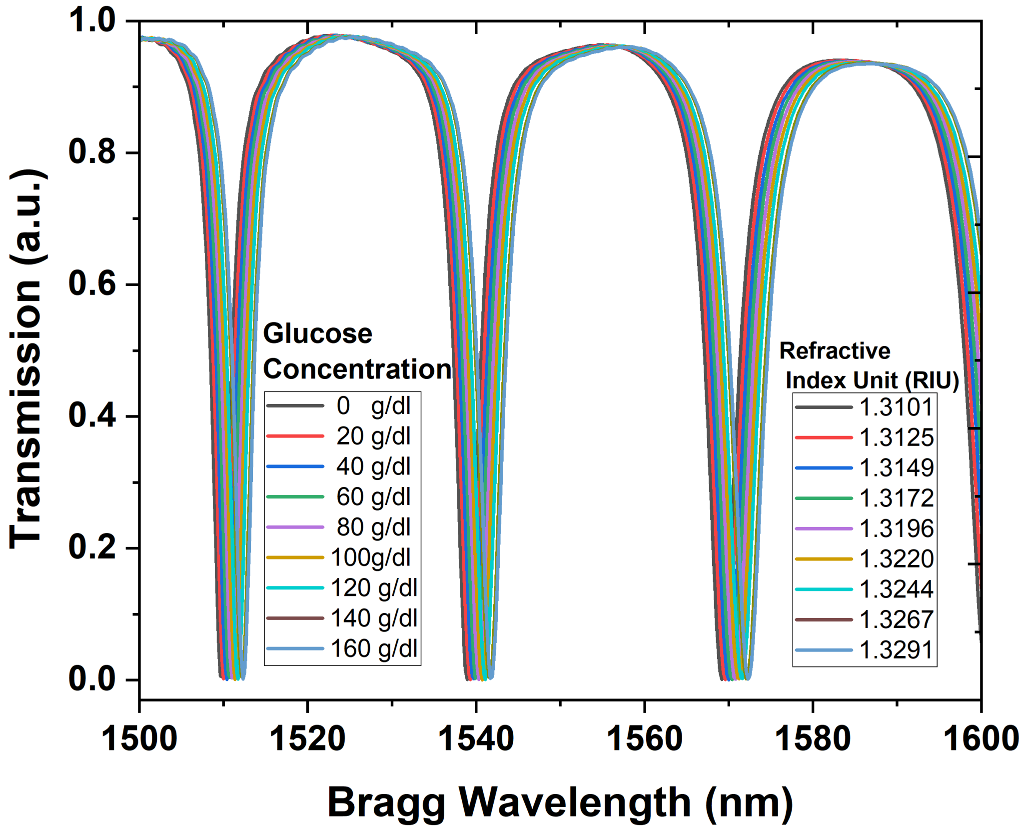

Figure 4.6: Transmission of glucose concentrations

Figure 4.7 shows the resonant wavelength for 0 g/dl was around 1539 nm but this is gradually increasing with every 20 g/dl such that at the highest concentration, 160 g/dl the wavelength is around 1542 nm. It can be concluded that the higher concentrations with a large refractive index caused a larger shift in the wavelength. It is this shift in wavelength that is important to calculate the sensitivity of the microring resonator.

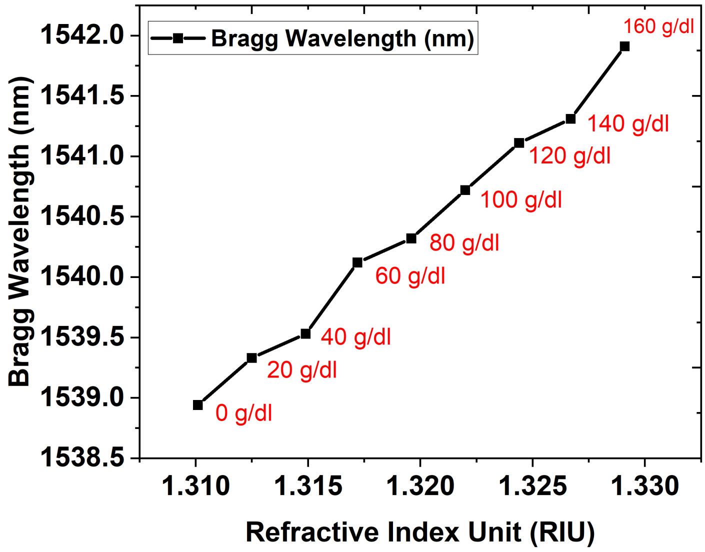

Figure 4.7: Resonant Wavelength vs Refractive Index Units

Figure 4.8 shows the overall sensitivity of the glucose sensor. The sensitivity of the microring resonator was obtained by using the eqn (2.7). The sensitivity value was found to be 155.24 nm/RIU. This value is higher than other experimental values, implying that the ring resonator sensor is indeed suitable for sensing applications.

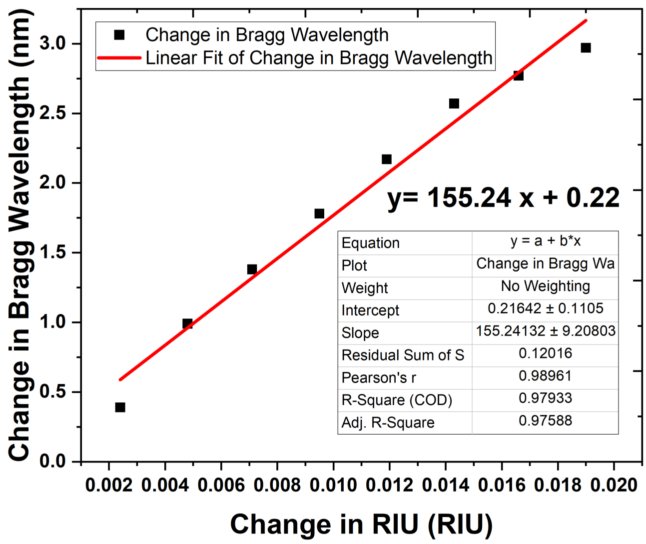

Figure 4.8: Sensitivity of glucose sensor

Figure 4.9 shows the sensitivity, figure of merit and quality factor at each glucose concentration level. At 20 g/dl glucose was introduced into the sensors environment causing a sharp increase. The sensors overall figure of merit was found to 51.7 by using eqn (2.8).

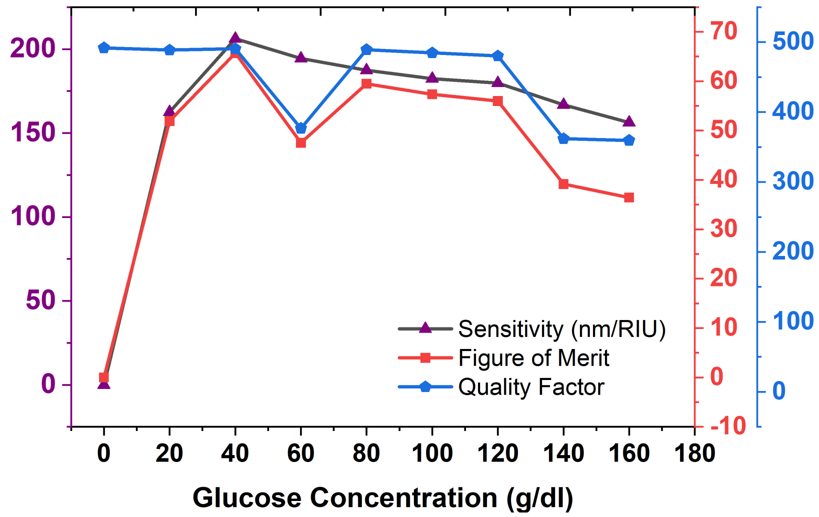

Figure 4.9: Sensitivity, Q-factor, Figure of Merit and Glucose concentration

Table 4.1 shows the sensitivity and q-factor of this study compared with those obtained from other studies. It is notable that this study has a high sensitivity. However, the q-factor is low compared to [14].

Table 4.1: Comparison of Sensitivity and Q-factor with other studies

Paper	**Sensitivity (nm/RIU)**	**Quality Factor**
C. Ciminelli et al.[9]	120	
A. Aransa et al. [2]	79.7	–
A. Aransa et al. [2]	70.32	–
Nuhogro et al. [14]	69.44	3385.31
T. Claes et al. [10]	298	330
This study	155.24	444.96

Chapter 5

Conclusion

In this study, a microring resonator biosensor has been designed for detecting the glucose concentration levels. Different concentrations of glucose which range from 0-160 g/dl is considered to study the performance of the sensor. A sensitivity value of 155 nm/RIU is revealed which is and Q-factor of 446. A modified design may lead to a higher quality factor value. However, the obtained results indicate that the microring resonator based biosensor has the ability to detect low glucose levels, as low as 1.3101 g/dl and detect resonance shift for every glucose concentration increment. Therefore, the designed glucose sensor can be hardware implemented for biosensing applications.

Bibliography

[1] Administrator. What are Biosensors? Principle, Working, Types and Applications — electronicshub.org, 2019. [Accessed 29-09-2023].

[2] Ananda Aransa, Lilik Hasanah, Cahya Julian, Roni Sumantri, Harbi Setyo Nugroho, Ahmad Aminudin, Roer Eka Pawinanto, Ahmad Rifqi MD Zain, Siti Kudnie Sahari, and Budi Mulyanti. Simulation microring resonator based on racetrack-shaped configuration for glucose sensing. *Journal of Engineering Science and Technology*, 15(5):2939–2949, 2020.

[3] Yash R Bawankar and Anamika Singh. Microring resonators based applications in silicon photonics-a review. In *2021 5th Conference on Information and Communication Technology (CICT)*, pages 1–6. IEEE, 2021.

[4] Ahlem Benmerkhi, Amel Bounouioua, Mohamed Bouchemat, and T. Boumaza. Analysis of a photonic crystal temperature sensor based on z-shaped ring resonator. *Optical and Quantum Electronics*, 53, 01 2021.

[5] Wim Bogaerts, Peter De Heyn, Thomas Van Vaerenbergh, Katrien De Vos, Shankar Kumar Selvaraja, Tom Claes, Pieter Dumon, Peter Bienstman, Dries Van Thourhout, and Roel Baets. Silicon microring resonators. *Laser & Photonics Reviews*, 6(1):47–73, 2012.

[6] Betty Butterfly. Microresonators: Configurations and Applications — findlight.net, 2022. [Accessed 27-09-2023].

[7] Linxuan Chen, Zilong Wang, and Zishuo Wang. Introduction of ic manufacturing to amateurs. In *SHS Web of Conferences*, volume 174, page 03003. EDP Sciences, 2023.

[8] Ioannis Chremmos, Otto Schwelb, and Nikolaos Uzunoglu. *Photonic microresonator research and applications*, volume 156. Springer, 2010.

[9] C. Ciminelli, F. Dell'Olio, D. Conteduca, C.M. Campanella, and M.N. Armenise. High performance soi microring resonator for biochemical sensing. *Optics Laser Technology*, 59:60–67, 2014.

[10] Tom Claes, Jordi Girones Molera, Katrien De Vos, Etienne Schacht, Roel Baets, and Peter Bienstman. Label-free biosensing with a slot-waveguide-based ring resonator in silicon on insulator. *IEEE Photonics journal*, 1(3):197–204, 2009.

[11] Stevanus Darmawan. *Microring resonator based photonic devices using high-contrast waveguides*. PhD thesis, 2009.

[12] Ecole Polytechnique Federale de Lausanne. A low-energy optical circuit for a new era of technology — phys.org, 2014. [Accessed 27-09-2023].

[13] Banshi Dhar Gupta, Roli Verma, and Sachin Kumar Srivastava. *Fiber optic sensors based on plasmonics*. World Scientific, 2015.

[14] Lilik Hasanah, Harbi Setyo Nugroho, Chandra Wulandari, Budi Mulyanti, Dilla Duryha Berhanuddin, Mohamad Hazwan Haron, P Susthitha Menon, Ahmad Rifqi Md Zain, Ida Hamidah, Khairurrijal Khairurrijal, et al. Enhanced sensitivity of microring resonator-based sensors using the finite difference time domain method to detect glucose levels for diabetes monitoring. *Applied Sciences*, 10(12):4191, 2020.

[15] Muzammil Iqbal, Martin A Gleeson, Bradley Spaugh, Frank Tybor, William G Gunn, Michael Hochberg, Tom Baehr-Jones, Ryan C Bailey, and L Cary Gunn. Label-free biosensor arrays based on silicon ring resonators and high-speed optical scanning instrumentation. *IEEE Journal of selected topics in quantum electronics*, 16(3):654–661, 2010.

[16] Steven G Johnson. Notes on perfectly matched layers (pmls). *arXiv preprint arXiv:2108.05348*, 2021.

[17] Venus Kohli. Semiconductor fabrication process: The ultimate guide to creating cutting-edge electronics, 2023. 14 January, 2024.

[18] Avinash P Nayak, VJ Logeeswaran, and M Saif Islam. Wet and dry etching. *University of California, California*, 2011.

[19] Payam Rabiei, William H. Steier, Cheng Zhang, and Larry R. Dalton. Polymer micro-ring filters and modulators. *J. Lightwave Technol.*, 20(11):1968, Nov 2002.

[20] EK Sharma, JP Nath, and N Dhingra. Coupled mode theory and coupled mode photonic devices: a review. *Asian J. Phys.*, 30:1–18, 2021.

[21] Patrick Steglich, Dominik G Rabus, Cinzia Sada, Martin Paul, Michael G Weller, Christian Mai, and Andreas Mai. Silicon photonic micro-ring resonators for chemical and biological sensing: A tutorial. *IEEE sensors journal*, 22(11):10089–10105, 2021.

[22] Yuze Sun and Xudong Fan. Optical ring resonators for biochemical and chemical sensing. *Analytical and bioanalytical chemistry*, 399:205–211, 2011.

[23] Vien Van. *Optical microring resonators: theory, techniques, and applications*. CRC Press, 2016.

[24] Eun-Hyung Yoo and Soo-Youn Lee. Glucose biosensors: an overview of use in clinical practice. *Sensors*, 10(5):4558–4576, 2010.